Soft Matter



View Article Online

PAPER



Cite this: Soft Matter 2020 **16**, 5273

Received 2nd March 2020, Accepted 10th May 2020

DOI: 10.1039/d0sm00371a

rsc.li/soft-matter-journal

Microfluidic rheology of methylcellulose solutions in hyperbolic contractions and the effect of salt in shear and extensional flows†

Benjamin L. Micklavzina, D. Athena E. Metaxas D. and Cari S. Dutcher D*

Methylcellulose solutions are known to form microfibrils at elevated temperatures or in the presence of salt. The fibrils have a significant impact on the solution's rheological properties. Here, the shear and extensional properties of methylcellulose solutions with added salt are measured using hyperbolic microfluidic channels, allowing for new characterization at lower molecular weights and higher shear and strain rates that are difficult to access by macroscale rheology studies. 1 and 2 wt% methylcellulose solutions with molecular weight of 150 kg mol⁻¹ with NaCl content between 0 to 5 wt% have been characterized. All solutions were found to be shear thinning, with power law thinning behavior at shear rates above 100 s⁻¹. The addition of NaCl up to 5 wt% had only small effects on shear viscosity at the shear rates probed (100 s⁻¹ and 10 000 s⁻¹). Extensional viscosities as low as 0.02 Pa s were also measured. Unlike the results for shear viscosity, the addition of 5 wt% NaCl caused significant changes in extensional viscosity, increasing by up to 10 times, depending on extension rate. Additionally, all solutions tested showed apparent extensional thinning in the high strain rate regime (>100 s⁻¹), which has not been reported in other studies of methylcellulose solutions. These findings may provide insight for those using methylcellulose solutions in process designs involving extensional flows over a wide range of strain rates.

Introduction

Converging geometries and extensional flows are present in many important industrial processes and geometries from inkjet printing and extrusion to nozzle and cross-slot geometries. 1-3 While a variety of approaches exist to study the rheological properties of complex liquids in extensional flows, 3,4 standard macroscale techniques are limited in the deformation rates and viscosities accessible. One of the more difficult flow regimes to probe involves dilute polymer solutions of low extensional viscosity (e.g., <100 mPa s), low polymer relaxation time (e.g. <1 ms), or high strain rate (e.g. $>1000 \text{ s}^{-1}$). For this reason, there has been increased interest in using microfluidic platforms to study extensional flows, since the microscale characteristic length scales allow users to probe fluids in these low fluid viscosity, high flow rate conditions simply and reliably.3,5-8

Methylcellulose (MC), a water-soluble food grade branched polymer, is used in a variety of commercial and scientific applications. MC-containing aqueous solutions demonstrate interesting rheological behavior, transitioning reversibly from

Department of Mechanical Engineering, University of Minnesota, 111 Church St SE, Minneapolis, MN, 55455, USA, E-mail: cdutcher@umn.edu

a liquid to a gel at elevated temperatures or in the presence of salts due to the formation of condensed microfibrils in solution.9-11 Using a macroscale capillary breakup extensional rheometer (CaBER), Morozova et al. 10 found that the extensional viscosity of methylcellulose solutions with molecular weight 530 kg mol⁻¹ and concentrations up to 1% by weight increased with the addition of NaCl, which is attributed to the presence of microfibrils dominating the apparent extensional properties of the solution. However, the CaBER approach could not characterize lower molecular weight solutions due to low relaxation times preventing formation of the elastocapillary bridge. Here, we use an alternative microfluidic-based method for measuring both shear and extensional viscosities for low molecular weight methylcellulose solutions.

For shear flows, some bulk techniques such as parallel plate geometries or Couette flows can reach high shear regimes, 12,13 though accurate analysis of viscometric data requires accounting for friction heating and resulting flow patterns. This makes a microfluidic approach to measuring shear viscosity appealing when probing higher shear rates. Microfluidic shear rheology generally involves the use of capillary rheometers, where the sample flows through a narrow rectangular channel.5 Measurements are made of the pressure drop across the channel as flow rates change, which can then be related to the fluid's shear

[†] Electronic supplementary information (ESI) available. See DOI: 10.1039/d0sm00371a

viscosity. Measurements of extensional viscosity in microfluidic setups, however, are more complex due to the presence of both shear and extension in these flows. Nonetheless, extensional viscosity can be isolated and measured in several ways in microfluidic channels, with geometries including cross slot flows, droplet breakoff, and hyperbolic contractions.³

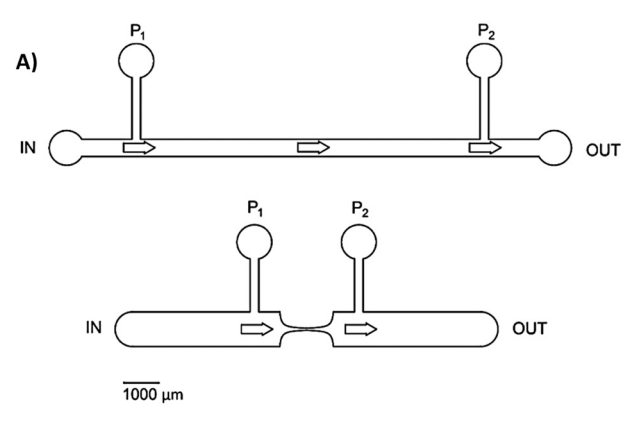
Cross slots in particular have been used to isolate and measure extensional properties of a variety of polymers, micellar solutions, and biological materials. 14-17 Extensional viscosities can be measured with this technique in several ways, though the most common methods involve measuring birefringence, particle trajectories, or pressure drops within the channel.15 The versatility of this technique makes it appealing for complex systems and has made it one of the leading techniques for extensional studies in microfluidics.

Hyperbolic contraction techniques are also attractive for studying extensional viscosity due to their ability to measure viscosity at a constant centerline extension rate and fixed total Hencky strain. In addition, measuring extensional viscosity with this technique is experimentally simple, needing only measurements of flow rate and pressure across the orifice. The range of strains and strain rates accessible differs between microfluidic techniques, with contractions often used for the highest extension rates (100-10000 s⁻¹) with relatively low Hencky strains ($\varepsilon_{\rm H} \sim 1$ –3). These kinds of devices are used to study extensional viscosity for single phase polymeric solutions as well droplet flows and emulsions. 18-20 Such microfluidic devices mimic processing conditions in industry settings and have already been used to study a variety of weakly viscoelastic fluids, including shampoos, aqueous polymer solutions, and micellar emulsions.5,7,21

In this study, the shear and extensional properties of low viscosity methylcellulose solutions containing fibrils are examined in the presence of varying concentrations of salt, and measurements of extensional viscosities at high shear and strain rates using hyperbolic contractions are presented. These results are compared with prior microfluidic work on similarly weak viscoelastic solutions to bring context to our findings for MC behavior. Finally, flow visualization through the hyperbolic contractions is shown via birefringence measurements to relate measured properties to fluid stresses. The work discussed here provides a clear method for studying low viscosity polymer solutions using a microfluidic setup and extends the range of understanding of methylcellulose solution properties in shear and extensional flows.

Materials and methods

PDMS channels are fabricated via soft lithography. In this method, the channel negatives are photopatterned onto a silicon wafer using SU8-2050 before being cured through heating. The resultant height of each channel is measured using a KLA-Tencor Surface Profilometer, with an average channel height of 120 µm. Polydimethylsiloxane mixed with accompanying cross-linker (Dow-Corning, SYLGARD 184) is prepared in a 10:1 ratio by weight and cured on this master wafer overnight



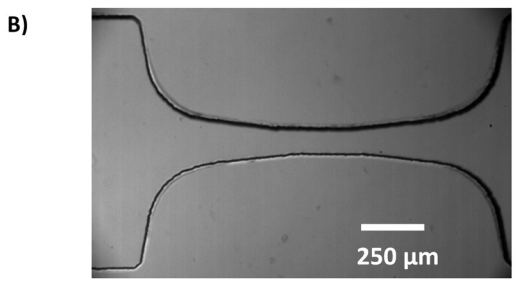


Fig. 1 Schematics (A) and image (B) of the microfluidic channels used to test shear and extensional viscosity. The schematics (A) represent a 20 mm long and 250 µm wide shear viscosity channel (top) and hyperbolic contraction channel for extensional viscosities (bottom). Also shown is a microscopy image (B) taken of the PDMS hyperbolic contraction shown in (A, bottom). The direction of flow in (A) is indicated by arrows. The pressure drop for both channels is found from measurements taken at the hydrostatic ports labeled P1 and P2

at 70 $^{\circ}$ C. Individual PDMS devices are then cut out and 1.25 mm diameter feed holes are punched into the ports shown in Fig. 1 located at the inlet, P₁, and outlet, P₂. Both the PDMS and the glass slide it is mounted onto are cleaned with methanol, isopropanol, and distilled water before undergoing an oxygen plasma treatment in a Harrick Plasma Cleaner (PDG-32G) for a minimum of 30 s. The plasma treatment allows the PDMS to bond to the glass surface, preventing leaks between the channel and the glass substrate.

To prepare the MC solutions, HPLC grade chromatography water was heated to 60 °C. For a 50 g total solution of MC, approximately 25 g of the HPLC grade water at 60 °C was added to the appropriate mass of MC powder and NaCl and stirred for 10 min. The remaining quantity of water at room temperature was added to the solutions and stirred for 10 min. Finally, the solutions were placed into an ice bath and stirred for an additional 10 min. After the preparation of the MC solutions, they were placed into a refrigerator at 2 °C for at least 24 h prior to use and were stored in the refrigerator when not in use. Prior to any experiments, the solutions were removed from the refrigerator and annealed at room temperature for 24 h.

The addition of salt in sufficient concentrations is known to cause both the formation of fibrillar structures and gelation in methylcellulose solutions (see Fig. 1 in ref. 12 for a schematic of the fibril structure). 9,10,22,23 Temperature-controlled small amplitude

oscillatory shear (SAOS) rheology taken for complex modulus G^* demonstrates thermoreversible gelation for both 1 wt% and 2 wt% of 150 kg mol⁻¹ methylcellulose in solution (MC150) and NaCl salt concentrations up to 8 wt%. The presence of salt causes gelation at lower temperatures, and at 8 wt% the salt induced gelling at 20 °C, which is the temperature of the experiments performed here. Based on these SAOS results, an upper salt concentration of 5 wt% was determined for the contraction experiments. This concentration allows for the possibility of fibril formation while keeping the solutions fluid (not gelled) during flow. Experimental results for the complex shear modulus of our MC150 solutions as a function of temperature and salt concentration can be found in Fig. S1 (ESI†) of the appendix.

All bulk rheology experiments were performed using a TA Instruments AR-G2 rheometer. Steady shear rheology experiments used a 2° steel 40 mm cone and plate geometry with a Peltier plate for heating. The viscosity was measured after the torque values reached an equilibrium state for each shear rate ranging from 0.1 to 1000 s⁻¹. The temperature was kept constant at 20 °C for all steady state shear experiments. Oscillatory shear rheology experiments were measured using a cup and bob geometry from 5 $^{\circ}$ C to 80 $^{\circ}$ C and back at a ramp rate of 1 °C min⁻¹ and angular frequency of 1 rad s⁻¹ at 1% strain. The outer diameter of the rotor was 14 mm, the rotor height was 42 mm, the cup's inner diameter was 15 mm, and the gap height was 5 mm. To prevent evaporation of the solutions during the temperature ramps, a thin layer of silicone oil (Sigma Aldrich, 5 cSt, density 0.963 g mL⁻¹, boiling point >140 °C) was floated on top of the solution. 24 The opening at the top of the cup and bob geometry was also covered with metal plates. These conditions were selected to match those used by Morozova et al. to characterize solutions of MC530.¹⁰ Steady shear rheometry was performed using the cone and plate geometry for MC solutions between shear rates of 0.1 s⁻¹ and 1000 s⁻¹, which overlaps with the shear rate range accessible with the microfluidic measurements, to verify the numerical accuracy of the results for samples in the lower shear rate regimes of this work. These results are displayed in Fig. S2 in the ESI† section.

For shear viscosity experiments, straight channels such as the one shown in Fig. 1A were used. The channel widths are either 250 µm or 500 µm and the channel lengths vary between 5 mm and 20 mm depending on the expected viscosity of the sample and the tolerance of the pressure sensor. It was found that results between channels of varied dimensions were indistinguishable so long as the pressure limits of the sensor were not exceeded. The flow of MC solutions is driven by a Harvard Apparatus Pro 11 Elite syringe pump at fixed flow rates up to 0.15 mL min⁻¹ while the pressure drop between points P₁ and P₂ was measured. The pressures were measured by connecting the P1 and P2 outlets to a 26PC15SMT Honeywell Wet/Wet Differential Pressure Sensor rated for 15 psi measurements. The sensors were initially calibrated by measuring the relative pressure differences between the hydrostatic reservoirs of varied lengths, using water and several Newtonian mixtures of glycerol

and water. For each trial, measurements are taken from the highest flow rate to the lowest flow rate, to avoid fluctuations that were found when low flow rates were used initially. An equilibration time of at least 10 min was given to allow pressure readings to stabilize at the sensor, though equilibration times as long as 20 min were sometimes used for more viscous samples. The need for such long equilibration times is likely due to a combination of factors in our setup, including long sensor channel tubing (60-70 cm), differences in fluid viscosity, and varying ranges of flow rates between fluid samples. Uncertainties in pressure readings were calculated using the minimum measurable pressure intervals (~200 Pa) and variation over time (repeated measurements over the course of 1 min).

For extensional viscosity measurements, a similar procedure was followed using the design featured in the bottom of Fig. 1A and B. In this case, the geometry of the channel is defined by the hyperbolically changing width

$$W(x) = \frac{1}{\frac{1}{W_0} + Bx}$$
 (1)

where the geometric factor here is $B = 20 \times 10^{-6} \, \mu \text{m}^{-1}$ and the initial channel width is $W_0 = 1$ mm. The contraction length (L_c) was set at 770 µm. Similar to the shear viscosity experiments, 10 to 15 min equilibrium times were used to allow flows to stabilize before pressures were recorded. Fluids were not recycled in either the shear or extensional techniques to avoid rheological changes due to flow history. Contraction experiments were first done using water to obtain an extensional viscosity. This extensional viscosity was later used to normalize results for

This extensional viscosity the relation $\eta_{\rm e} = \frac{4\eta_{\rm shear,water}}{\eta_{\rm e,water}} \eta_{\rm measured}$.

To check the plausibility of this method, experiments were performed with a 50/50 glycerol mixture. The resulting Trouton ratio was found to be 3.9 \pm 0.4, which is plausibly similar to the expected value of 4 for planar extension.²⁵

For the 1 wt% MC solutions, the Reynolds numbers tested in the contraction center $\left(\text{Re} = \frac{2\rho W_{\text{c}} H L_{\text{c}} \dot{\epsilon}}{\eta_0(W_{\text{c}} + H)} \right)$ spanned the orders of $\sim 10^{-3}$ -1 and the elasticity numbers $\left(\text{El} = \frac{\lambda \eta_0(W_{\text{c}} + H)}{2\rho L_{\text{c}} W_{\text{c}} H} \right)$

were on the order of $\sim 10-10^2$. Similarly, the 2 wt% MC solutions were tested at Reynolds numbers ranging over $\sim 10^{-3}$ - 10^{-2} and elasticity numbers on the order of 10^2 . Here η_0 is the shear viscosity at the lowest measured shear rate, W_c is the width of the channel at the contraction center, H is the channel height, λ is the fluid relaxation time estimated between 30–100 ms from G' and G'' measurements, ρ is the fluid density, and $\dot{\epsilon}$ is the shear rate. With elasticity numbers greater than 10 and Reynolds numbers on the order of 1 at most, stretching effects should be more influential than inertial effects on

Visualization of flows via birefringence was performed separately from the pressure drop experiments, using the same contraction geometry shown in Fig. 1 (bottom). In this case, a setup like that of Sun and Huang²⁹ was employed involving a

flow. 5,26-28

rotating polariscope with the first 1/4 waveplate fixed at 45° and the second 1/4 waveplate fixed at -45° with respect to the analyzer. A diagram of this setup can be found in Fig. 2. In this method, an initial reference image was taken of the light intensity incident on the sample, I_0 . This intensity was later compared to the transmitted intensity, I, when both the second 1/4 waveplate and the analyzer were in place. The relative intensity of light at each point can then be related to the sample retardance, δ , by the relation²⁹

$$\frac{I}{I_0} = \sin^2 \frac{\delta}{2} \tag{2}$$

The apparent retardance at a given flow rate is normalized by subtracting the signal at zero flow.

All birefringence measurements were performed using a single device to minimize the effects of differences in PDMS on apparent retardance. To increase the channel wall stiffness and minimize their birefringent response, a ratio of PDMS to cross-linker of 5:1 by weight was used. Also, to increase the sensitivity of the FastCam Mini AX200 to the changes in transmitted intensity due to birefringence, the initial reference image and the measurement image were taken at different exposure times. The ratio of these exposure times between the reference and the measurement was 1/6400 s:1/50 s, with these fractions corresponding to frame rates in the camera. Flows were given a minimum of 5 min to equilibrate for these

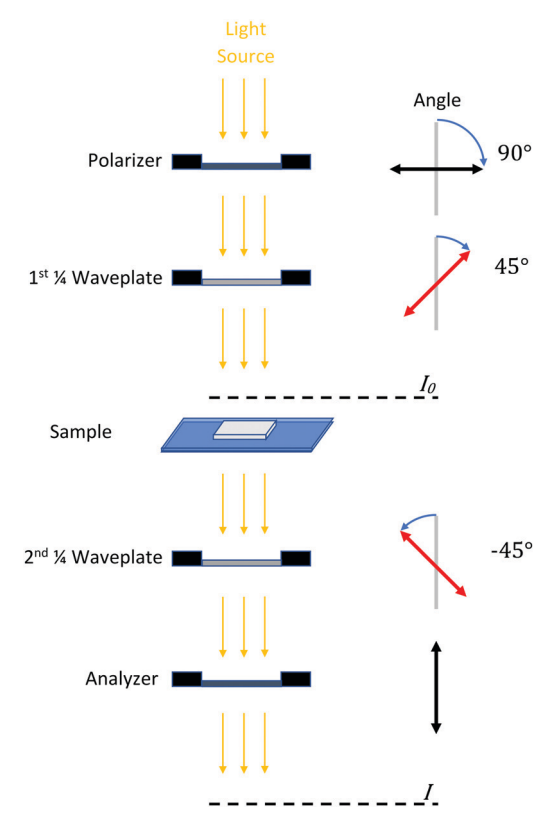


Fig. 2 Above is a diagram of the birefringence setup used to measure and map sample retardance. Shown are I, the transmitted light intensity, and I_0 the light intensity incident on the sample

trials, which is slightly less than previous times from the pressure drop measurements due to the high flow rates (i.e., high sample volumes) required to observe large sample retardance. For these reasons, the results and comparisons between the pressure measurements and the birefringence measurements should be considered qualitative.

Before taking measurements, the birefringent response of PDMS to pressure was determined. Using a 50/50 glycerol/water solution, which is known to have no birefringent properties, a retardance change of $\sim 10^{-5} \text{ kPa}^{-1}$ could be observed at the side walls of the channel, though little effect could be seen in the channel center.

Results and discussion

Shear microfluidic rheology: theory

To determine the extensional viscosity of a fluid flowing through a hyperbolic contraction, the shear viscosity must first be determined. In the extensional viscosity calculations, three components must be known: (a) the viscous losses in the channel leading up to the contraction, (b) the viscous losses across the contraction itself, and (c) the extensional losses across the contraction. Both the viscous losses in the precontraction channel and in the contraction itself depend on the shear viscosity dependence on shear rate. The total pressure drop across the contractions is thus

$$\Delta P_{\text{measured}} = \Delta P_{\text{channel}} + \Delta P_{\text{viscous}} + \Delta P_{\text{extension}}.$$
 (3)

Once $\Delta P_{\text{extension}}$ is known, then an extensional viscosity can be calculated using the relation

$$\eta_{\rm E} = \frac{\Delta P_{\rm extension}}{\dot{\varepsilon}\varepsilon_{\rm H}} = \frac{\Delta P_{\rm extension}H}{QB\ln\left(\frac{W_0}{W_c}\right)},$$
(4)

where H is the channel height, Q is the flow rate in the channel, W_0 is the width of the channel at the beginning of the contraction, W_c is the channel width at the center of the contraction, ε_H is the Hencky strain, and $\dot{\varepsilon}$ is the extensional strain rate, assuming the rate of strain follows the relation $\dot{\varepsilon} = \frac{Q}{H}B$. If one measures the total pressure loss across the contraction and estimates the viscous losses between the sensor channels, then extensional viscosity can be determined.

However, estimating viscous losses for the $\Delta P_{\text{viscous}}$ and $\Delta P_{\text{channel}}$ terms in eqn (3) requires knowledge of how the shear viscosity changes with the shear rate in the channels. It is this step that is often the most challenging. To determine this for the MC solutions, the pressure drop along rectangular channels (Fig. 1A, top) at different flow rates was measured. The pressure drop in a rectangular channel is related to the shear viscosity by the equation 1

$$\eta = \frac{WH\Delta P}{L(W+H)} \frac{1}{\dot{\gamma}_{w}} \tag{5}$$

where ΔP is the pressure loss in the channel, W is the channel width, H is the channel height, L is the channel length, and $\dot{\gamma}_{\rm w}$ is the shear rate at the wall. For a Newtonian fluid the shear rate at the

walls is defined by

$$\dot{\gamma}_{\rm w} = \dot{\gamma}_{\rm a} = \frac{6Q}{WH\left(\frac{WH}{W+H}\right)} \tag{6}$$

where $\dot{\gamma}_a$ is considered an apparent shear rate for a fluid with a parabolic flow profile. For fluids with shear dependent properties, flow in the channel is generally non-parabolic and requires use of the Weissenberg–Rabinowitsch correction for rectangular channels. This corrected shear rate term can be expressed as

$$\dot{\gamma}_{w} = \frac{\dot{\gamma}_{a}}{3} \left(2 + \frac{d \ln \dot{\gamma}_{a}}{d \ln \tau_{R}} \right) \tag{7}$$

where τ_R is the shear at the wall. It should be noted here that in the case of a Newtonian fluid, the term $\frac{d \ln \dot{\gamma}_a}{d \ln \tau_R} = 1$, and the result reduces to that of eqn (6). In terms of measurable variables, the corrected eqn (5) can be converted to the form

$$\eta = \frac{WH\Delta P}{L(W+H)} \frac{WH\left(\frac{WH}{W+H}\right)}{2Q\left(2 + \frac{\Delta P}{Q}\frac{dQ}{d\Delta P}\right)}$$
(8)

Shear microfluidic rheology: measurements

Thus, measuring shear viscosities in the rectangular channels requires only that we measure ΔP across a channel of known dimensions W, H, and L as a function of Q. To verify the pressure measurements, Newtonian fluids with known shear viscosities were measured (Fig. 3A). The shear viscosities of both water and two glycerol/water solutions by volume are nearly constant with shear rate. The pressure sensor was calibrated so that the average shear viscosity for water was equal to that of water at 20 °C at 1.0×10^{-3} Pa s. With this in mind, the measured shear viscosity of the 50:50 glycerol/water mixture was found to be 8.8×10^{-3} Pa s. This compares well with the expected value from literature of 8.4×10^{-3} Pa s, 29 with an error of roughly 5% present in these results. While the 75:25 glycerol/water mixture appears similarly Newtonian, it

deviates more from literature values with a measured shear viscosity of 45×10^{-3} Pa s compared to the literature value at 20 °C of 55×10^{-3} Pa s. This error may be due to temperature variations in the lab; however, the measured value falls within 5 °C of the literature viscosity.

For the shear-thinning MC150 solutions shown in Fig. 3, shear thinning can be seen at shear rates greater than $\sim\!100~\rm s^{-1}$ regardless of the amount of MC150 dissolved. In the shear thinning regime, the solutions behave similarly to a power law fluid with constitutive equation

$$\eta = m\dot{\gamma}_{\rm w}^{n-1} \tag{9}$$

where m and n are fitted scalar values specific to the fluid, and n < 1 for shear thinning solutions. The values of m and n at the highest shear rates for the MC150 solutions tested are given in Table 1. Power law fits in this table were done using all data points from shear rates greater than 300 s⁻¹ so as not to include the low shear plateau. In the range of shear rates observed, little difference was found between the shear viscosities of 1 wt% MC150 with and without added NaCl. Values of the exponent nat high shear rates were found to be a nearly identical at n = 0.66, and the magnitude of shear viscosities observed for these lower MC150 concentrations was 0.05 Pa s at the low shear plateau. For 2 wt% MC150 solutions, the addition of salt does not appear to cause significant changes to the power law exponent. Values ranged from 0.57 \pm 0.01 for the solution with 5 wt% NaCl to 0.62 \pm 0.03 for the solution with 4 wt% NaCl. The viscosity at lower shear rates showed some dependence on NaCl concentration, with the plateau shear viscosity going from 0.44 Pa s without salt to 0.58 Pa s at an NaCl concentration of 5 wt% and a shear rate of 40 s⁻¹. For comparison, Morozova et al. found that 1 wt% MC530 solutions had power law thinning for shear rates greater than $\sim 10 \text{ s}^{-1}$, and the power law exponent in the high shear regime was 0.33 for no NaCl present and 0.55 in 8 wt% NaCl. 10 They similarly observed a change in transition behavior upon the addition of salt, which included a characteristic increase in the shear viscosity and the replacement of the Newtonian regime with a shear thinning regime at low shear rates. The effect of salt on the low shear

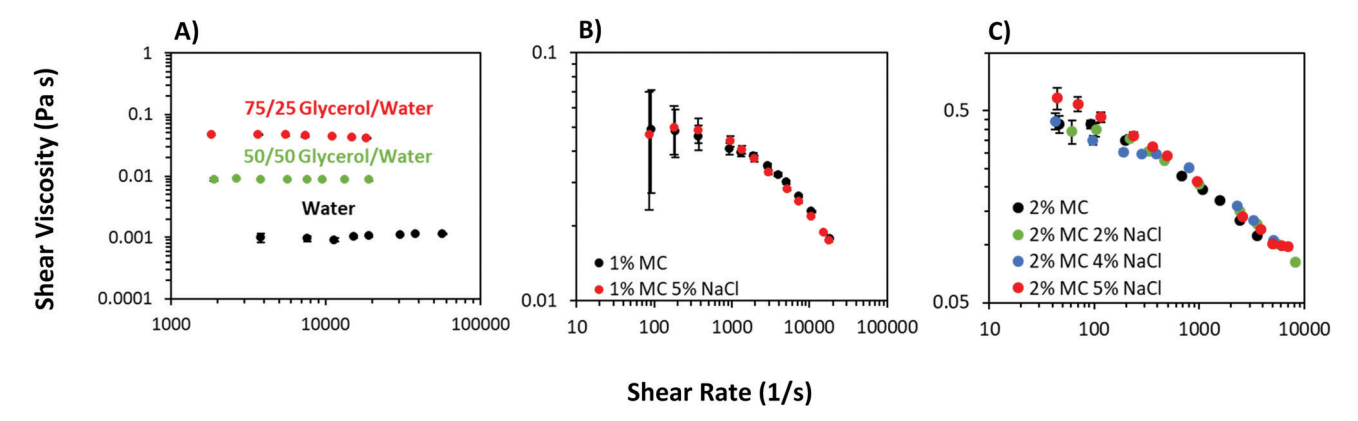


Fig. 3 Measured shear viscosities for Newtonian fluids and MC solutions using microfluidic hyperbolic contractions in the presence of added salt. Shown in (A) are results for water and two glycerol/water Newtonian mixtures. Ratios given are by volume. Results for (B) 1 wt% MC150 and (C) 2 wt% MC150 solutions from slit rheometry are also shown. Error bars represent a variance due to limitations of the pressure sensor.

Paper Soft Matter

Power law indices for MC solutions

MC concentration (wt%)	Salt concentration (wt%)	m (Pa s ^{n})	n
1	0 5	$\begin{array}{c} 0.43 \pm 0.07 \\ 0.46 \pm 0.05 \end{array}$	$\begin{array}{c} 0.68 \pm 0.02 \\ 0.67 \pm 0.01 \end{array}$
2	0 2 4 5	3.9 ± 0.4 3.2 ± 0.3 2.9 ± 0.7 4.2 ± 0.3	$\begin{array}{c} 0.59 \pm 0.01 \\ 0.60 \pm 0.01 \\ 0.62 \pm 0.03 \\ 0.57 \pm 0.01 \end{array}$

regime is thought to be due to the presence of fibrils, which is consistent with expectations from bulk rheology testing. While the shear measurements in this work were performed to inform the extensional viscosity measurements in the following sections, it should be noted that the results obtained here extends the range of available measurements for MC solutions to higher shear rates $(1000 \text{ s}^{-1} \text{ to } 10000 \text{ s}^{-1})$ than those obtained previously using bulk techniques for MC530.¹⁰

Contraction experiments: theory

As mentioned earlier, the extensional viscosity for these solutions is measured by finding the pressure drop across the contraction setups from Fig. 1. Using this technique to measure extensional viscosity requires determining two terms associated with viscous contributions: one for losses in the rectangular channel region between the sensor ports, $\Delta P_{\text{channel}}$, and one associated with the contraction itself, $\Delta P_{\rm viscous}$. The first of these terms can be easily deduced using eqn (8) and shear viscosity data from Fig. 3, but the second term is generally difficult to discern. A commonly applied method of calculating the viscous losses in the contraction is given by the lubrication approximation for a power law fluid, 5,30 with the primary result being of the form

$$\Delta P_{\text{viscous}} = \frac{2^{n+2}}{n+1} \left(\frac{2n+1}{n}\right)^n \left(\frac{L_c}{H}\right)^{n+1} \times \left(\left(\frac{W_0}{W_0 - W_c}\right)^{n+1} - \left(\frac{W_c}{W_0 - W_c}\right)^{n+1}\right) m \dot{\varepsilon}^n$$
(10)

where L_c is the length to the center of the contraction, W_0 is the channel width at the entrance to the contraction, W_c is the width at the narrowest point of the contraction, and $\dot{\varepsilon}$ is the rate of strain. Key to this approximation is the assumption that the width of the contraction channel is significantly larger than the height, which is not true for these devices near the contraction's center. However, contractions with ratios of W_c/H on the order of 1 have been used in conjunction with eqn (10) to estimate extensional viscosities in hyperbolic geometries. For example, Ober et al. used a contraction with $W_c = 400 \mu m$ and $H = 150 \mu m$ to characterize several industrial and commercial surfactant mixtures while applying the lubrication approximation.⁵ However, this approach is known to underestimate the viscous losses across hyperbolic contractions by roughly an order of magnitude, and is especially poor for setups with contraction ratios greater than 5-10.30 Indeed, for this setup the extensional viscosities of the Newtonian systems systematically overpredict the expected value from Trouton's ratio. Still, using this relation can provide some qualitative measure of how extensional properties change in mixed flows seen in many industrial processes by calibrating the reported extensional viscosities using the measured extensional viscosity of water.

Contraction experiments: measurements

The results of using eqn (10) in the determination of the extensional viscosity, recalibrated by the measured extensional viscosity of water, can be seen in Fig. 4. Here, it can be seen that the addition of NaCl leads to a significant increase in apparent extensional viscosity for the 2 wt% MC150 solutions while causing a much smaller change in the 1 wt% MC150 solutions. At low shear rates, the 2 wt% MC solutions without salt increase from an apparent extensional viscosity of 0.2-0.4 Pa s to roughly 0.9-1.2 Pa s at an NaCl concentration of 5 wt%. At higher shear rates, this trend remains but is less apparent, with the extensional viscosity at extension rate of 450 s^{-1} increasing from 0.24 Pa s without NaCl to 0.32 Pa s with 5 wt% NaCl. Like the results for shear viscosities, the effect of NaCl addition on extensional viscosity appears to be much smaller for the 1 wt% MC solutions than the 2 wt% solutions. The difference in extensional viscosity between the salt free and 5 wt% NaCl solutions was found to be highest at an extensional strain rate of $\sim 60 \text{ s}^{-1}$, with NaCl causing an increase from

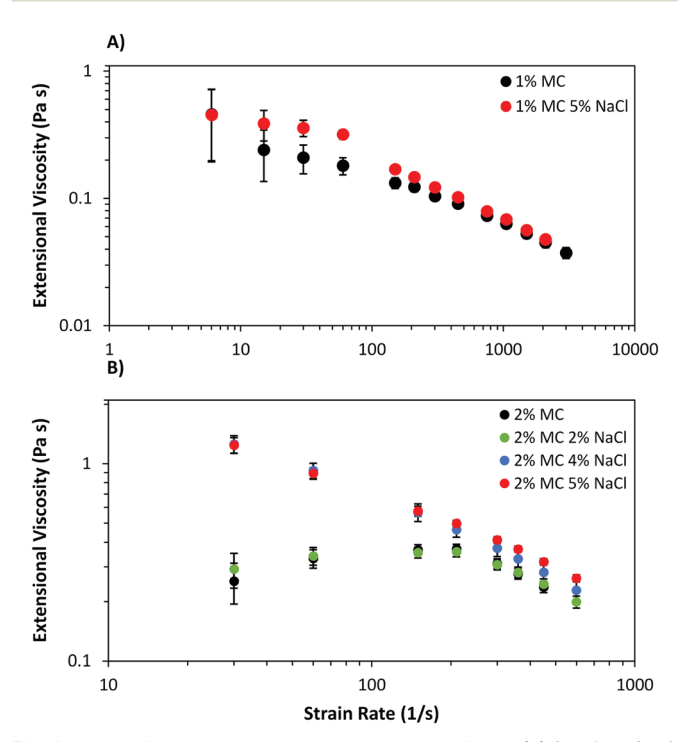


Fig. 4 In this figure, the extensional viscosities of both (A) 2 wt% MC150 and (B) 1 wt% MC150 solutions are plotted against extensional strain rate in the contraction. Viscosities were determined using the lubrication approximation in eqn (10) and the tabulated power law coefficients in Table 1.

Soft Matter

0.18 Pa s to 0.32 Pa s. Increasing extensional strain rate also appeared to decrease this difference in extensional viscosity for the 1 wt% MC150 solutions.

Additionally, extensional viscosities obtained with this method show an apparent trend of extensional thinning at higher strain rates. Initially, this result may be counterintuitive, as MC solutions are known to be extensional thickening fluids from prior work obtained at lower strain rates. 10 However, literature suggests that at higher strain rates this thinning behavior is expected for entangled and branched polymers in solution, such as guar and xanthan gum. 25,31-33 For MC150 solutions, the overlap concentration without salt has previously been both calculated and experimentally determined to be 0.21% by weight.24,34 Since the entanglement concentration is generally taken to be 5-10 times the overlap concentration, the solutions tested can be considered to be at or near concentrations at which molecular entanglements occur.35 The cause of this thinning behavior is thought to be tied to the loss of entanglements between and along polymer molecules.31 It is often accompanied by an initial rise in extensional viscosity, as seen with the 2 wt% MC150 with 0 and 2 wt% NaCl solutions, attributed to an elastic response from the polymer chains. Further discussion of the ratio of the extensional and shear viscosities with calculated apparent Trouton ratios using an equivalent deformation method is given in the ESI.†

Flow visualization

In addition to measured pressure drops for shear and extensional viscosities, birefringence visualization of optical retardance, δ , was also used to characterize the methylcellulose solutions in extensional flow fields. Birefringence is a property associated with anisotropy in indices of refraction for a given material. In polymer solutions this is typically a result of polymer alignment in the fluid, which results from fluid stresses increasing the alignment of adjacent molecules.

Retardance, which represents the phase difference accumulated between orthonormally polarized light waves travelling through the material, is generally used as a measure of stress response for such materials. The first normal stress difference, N_1 , and retardance can be related via the 2D stress optical law^{29,36}

$$\delta = \frac{2\pi HC}{\lambda} N_1 \tag{11}$$

where C is the stress optical coefficient, H is the channel height, and λ is the wavelength of light. While the simple relationship of eqn (11) breaks down at higher stresses, a greater value for N_1 is still expected to increase the optical response and measured retardance of the fluid. Retardance maps were made for each MC solution at high flow rates of 0.2 to 0.4 mL min⁻¹ to maximize the apparent signal (Fig. 5). An example of how these retardance maps vary along the centerline of the channel can be found in Fig. S3 of the ESI† section.

Centerline measurements of retardance for both 1 wt% MC150 and 2 wt% MC150 solutions show a strong dependence on flow rate, with peak retardance in the channel increasing from 3×10^{-3} at 0.1 mL min⁻¹ to 7×10^{-3} at 0.4 mL min⁻¹ for the 2 wt% MC150 in 5 wt% NaCl solution shown in Fig. S3 (ESI†). Interestingly, the presence of NaCl does not appear to have a major effect on the centerline retardance.

In addition to centerline cross sections, vertical slices for the 2 wt% MC150 solutions are given near the center of the contraction in Fig. S3B (ESI†). Similar to the centerline measurements, increasing flow rate causes a corresponding increase in retardance. However, there are two interesting features to these vertical patterns. The first is that there is a non-zero slope to the retardance in the channel, implying that flow is not symmetric across the centerline. The second interesting feature is the presence of a prominent peak in retardance at the edge of the channel. The height of this peak appears to be influenced by the presence of added NaCl, with the ratio of

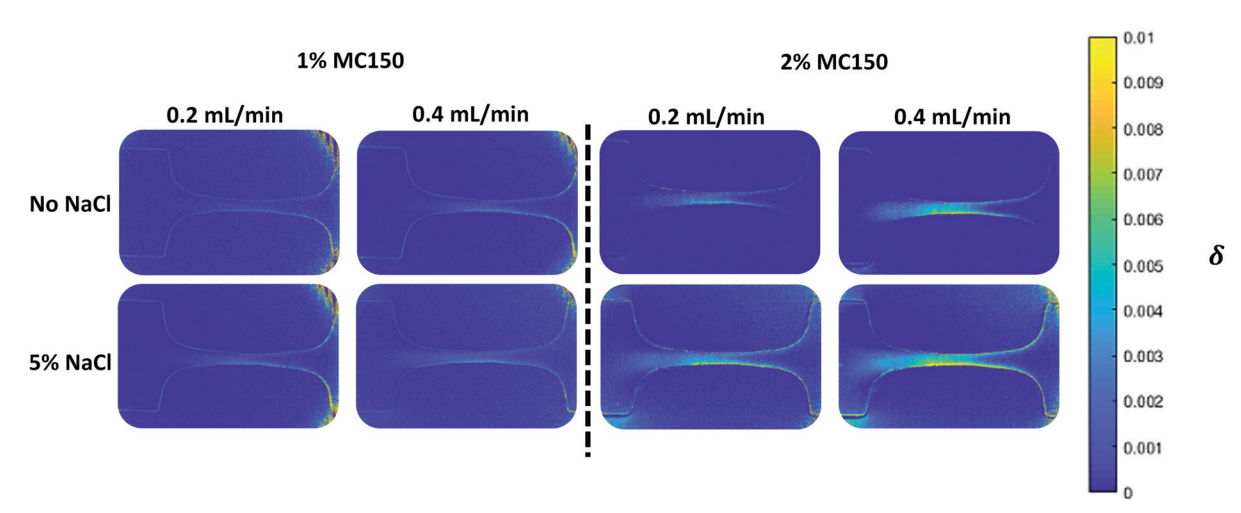


Fig. 5 Shown are retardance maps for (left) 1 wt% MC150 solutions and (right) 2 wt% MC150 solutions in the presence of added salt. Images were taken using a PDMS device with a 5:1 base to crosslinker ratio. Here we note that the retardance maps have some added signal at the walls due to the response of the PDMS rather than the fluid itself.

peak to minimum intensity increasing for 2 wt% MC150 from ~1.5 without NaCl to ~2.2 at 5 wt% NaCl. This trend continues for the 1 wt% MC150 solutions, with ratios increasing from \sim 3 without NaCl to \sim 4.3 at 5 wt% NaCl. While this trend is tied to differences in flow patterns, it is also likely that observed differences are an effect of fibrils on birefringent properties. It is understood from literature that, when there are structures within a fluid that have very different optical properties (such as micelles or fibrillar structures) from the bulk fluid, birefringent streaks can occur along paths of higher shear, 37,38 similar to that observed here in Fig. 5 and Fig. S3 (ESI†).

Conclusions

The work here uses microfluidic platforms to extend the knowledge of MC solution shear and extensional rheology up to shear and strain deformation rates of 10⁴ s⁻¹. The results match macro-scale results available at lower deformation rates and show that increased presence of fibrils leads to an increase in the extensional viscosity as expected. In addition, these results also appear to imply that methylcellulose solutions undergo extensional thinning past extension rates of 10-100 s⁻¹. The rheological characterization combined with the birefringence visualization presented here will enable enhanced understanding of MC solutions in flow and improve handling of MC solutions in high extension geometries or industrial processes such as nozzle or inkjet printing.

Conflicts of interest

There are no conflicts to declare.

Acknowledgements

This work was primarily supported by the National Science Foundation (NSF) through the University of Minnesota MRSEC under Award Number DMR-1420013. Part of this work was carried out in the Polymer Characterization Facility, University of Minnesota, which has received capital equipment funding from the NSF through the UMN MRSEC under Award Number DMR-1420013. Portions of this work were conducted in the Minnesota Nano Center, which is supported by the National Science Foundation through the National Nano Coordinated Infrastructure Network (NNCI) under Award Number ECCS-1542202. A. M. was supported through an NSF Graduate Research Fellowship.

Notes and references

- 1 C. W. Macosko, Rheology: principles, measurements, and applications, Wiley-VCH, 1996.
- 2 T. R. Tuladhar and M. R. Mackley, J. Non-Newtonian Fluid Mech., 2008, 148, 97-108.

- 3 F. J. Galindo-Rosales, M. A. Alves and M. S. N. Oliveira, Microfluid. Nanofluid., 2013, 14, 1-19.
- 4 J. M. Dealy, Polym. Eng. Sci., 1971, 11, 433-445.
- 5 T. J. Ober, S. J. Haward, C. J. Pipe, J. Soulages and G. H. McKinley, Rheol. Acta, 2013, 52, 529-546.
- 6 S. J. Haward, T. J. Ober, M. S. N. Oliveira, M. A. Alves and G. H. McKinley, Soft Matter, 2012, 8, 536-555.
- 7 L. Campo-Deaño, F. J. Galindo-Rosales, F. T. Pinho, M. A. Alves and M. S. N. Oliveira, J. Non-Newtonian Fluid Mech., 2011, 166, 1286-1296.
- 8 B. Keshavarz and G. H. McKinley, Biomicrofluidics, 2016, 10, 043502.
- 9 T. P. Lodge, A. L. Maxwell, J. R. Lott, P. W. Schmidt, J. W. McAllister, S. Morozova, F. S. Bates, Y. Li and R. L. Sammler, Biomacromolecules, 2018, 19, 816-824.
- 10 S. Morozova, P. W. Schmidt, A. Metaxas, F. S. Bates, T. P. Lodge and C. S. Dutcher, ACS Macro Lett., 2018, 7, 347-352.
- 11 J. R. Lott, J. W. McAllister, S. A. Arvidson, F. S. Bates and T. P. Lodge, Biomacromolecules, 2013, 14, 2484-2488.
- 12 C. J. Pipe, T. S. Majmudar and G. H. McKinley, Rheol. Acta, 2008, 47, 621-642.
- 13 N. C. Crawford, S. K. R. Williams, D. Boldridge and M. W. Liberatore, Rheol. Acta, 2012, 51, 637-647.
- 14 K.-W. Hsiao, C. Sasmal, J. R. Prakash and C. M. Schroeder, J. Rheol., 2017, 61, 151-167.
- 15 C. M. Schroeder, J. Rheol., 2018, 62, 371-403.
- 16 K.-W. Hsiao, J. Dinic, Y. Ren, V. Sharma and C. M. Schroeder, Phys. Fluids, 2017, 29, 121603.
- 17 J. A. Pathak and S. D. Hudson, Macromolecules, 2006, 39, 8782-8792.
- 18 M. Chellamuthu, E. M. Arndt and J. P. Rothstein, Soft Matter, 2009, 5, 2117-2124.
- 19 M. K. Mulligan and J. P. Rothstein, Phys. Fluids, 2011, 23, 022004.
- 20 S. G. Kim, C. M. Ok and H. S. Lee, J. Rheol., 2018, 62, 1261-1270.
- 21 G. H. McKinley, L. E. Rodd, M. S. N. Oliverira and J. Cooper-White, J. Cent. South Univ. Technol., 2007, 14, 6-9.
- 22 M. A. Villetti, V. Soldi, C. Rochas and R. Borsali, Macromol. Chem. Phys., 2011, 212, 1063-1071.
- 23 P. W. Schmidt, S. Morozova, P. M. Owens, R. Adden, Y. Li, F. S. Bates and T. P. Lodge, Macromolecules, 2018, 51, 7767-7775.
- 24 S. A. Arvidson, J. R. Lott, J. W. McAllister, J. Zhang, F. S. Bates, T. P. Lodge, R. L. Sammler, Y. Li and M. Brackhagen, Macromolecules, 2013, 46, 300-309.
- 25 D. M. Jones, K. Walters and P. R. Williams, Rheol. Acta, 1987, 26, 20-30.
- 26 P. Dontula, M. Pasquali, L. E. Scriven and C. W. Macosko, Rheol. Acta, 1997, 36, 429-448.
- 27 H. Zhang and K. Nishinari, Food Hydrocolloids, 2009, 23,
- 28 S. Różańska, L. Broniarz-Press, J. Różański, P. T. Mitkowski, M. Ochowiak and S. Woziwodzki, Food Hydrocolloids, 2013, 32, 130-142.

- 29 C.-L. Sun and H.-Y. Huang, Biomicrofluidics, 2016, 10, 011903.
- 30 H. S. Lee and S. J. Muller, J. Rheol., 2017, 61, 1049-1059.
- 31 S. Różańska, in Advances in Food Rheology and Its Applications, ed. J. Ahmed, P. Ptaszek and S. Basu, Woodhead Publishing, 2017, pp. 125-157.
- 32 M. D. Torres, B. Hallmark and D. I. Wilson, Food Hydrocolloids, 2014, 40, 85-95.
- 33 J. Meadows, P. A. Williams and J. C. Kennedy, Macromolecules, 1995, 28, 2683-2692.
- 34 T. Funami, Y. Kataoka, M. Hiroe, I. Asai, R. Takahashi and K. Nishinari, Food Hydrocolloids, 2007, 21, 46-58.
- 35 M. Rubinstein and R. H. Colby, Polymer physics, Oxford University Press, New York, 2003.
- 36 T. J. Ober, J. Soulages and G. H. McKinley, J. Rheol., 2011, **55**, 1127-1159.
- 37 N. Oba and T. Inoue, Rheol. Acta, 2016, 55, 699-708.
- 38 D. Hemsley, in Comprehensive Polymer Science and Supplements, ed. G. Allen and J. C. Bevington, Pergamon, Amsterdam, 1989, pp. 765-784.